



**HAL**  
open science

## Automatic generation of parallel and coherent code using the YAO variational data assimilation framework

Luigi Nardi, Julien Brajard, Sylvie Thiria, Fouad Badran, Pierre Fortin

### ► To cite this version:

Luigi Nardi, Julien Brajard, Sylvie Thiria, Fouad Badran, Pierre Fortin. Automatic generation of parallel and coherent code using the YAO variational data assimilation framework. 2016. hal-00783328v2

**HAL Id: hal-00783328**

<https://hal.sorbonne-universite.fr/hal-00783328v2>

Preprint submitted on 20 Jun 2016

**HAL** is a multi-disciplinary open access archive for the deposit and dissemination of scientific research documents, whether they are published or not. The documents may come from teaching and research institutions in France or abroad, or from public or private research centers.

L'archive ouverte pluridisciplinaire **HAL**, est destinée au dépôt et à la diffusion de documents scientifiques de niveau recherche, publiés ou non, émanant des établissements d'enseignement et de recherche français ou étrangers, des laboratoires publics ou privés.

# Automatic generation of parallel and coherent code using the YAO variational data assimilation framework

Luigi Nardi<sup>1,2</sup>, Julien Brajard<sup>1</sup>, Sylvie Thiria<sup>1</sup>, Fouad Badran<sup>2</sup> and Pierre Fortin<sup>3</sup>

<sup>1</sup> LOCEAN, Laboratoire d’Océanographie et du Climat: Expérimentations et approches numériques. UMR 7159 CNRS / IRD / Université Pierre et Marie Curie / MNHN. Institut Pierre Simon Laplace. 4, place Jussieu Paris 75005, France.

<sup>2</sup> CEDRIC, Centre d’Etude et De Recherche en Informatique du CNAM. EA 1395, 292 rue St Martin Paris 75003, France.

<sup>3</sup> Sorbonne Universités, UPMC Univ Paris 06, UMR 7606, LIP6, F-75005, Paris, France CNRS, UMR 7606, LIP6, F-75005, Paris, France

01/07/2016

## Abstract

Variational data assimilation estimates key control parameters of a numerical model to minimize the misfit between model and actual observations. YAO is a code generator based on a modular graph decomposition of the model; it is particularly suited to generating adjoint codes, which is the basis for variational assimilation experiments. We present an algorithm that checks the consistency of the calculations defined by the user. We then present how the modular graph structure enables an automatic and efficient parallelization of the generated code on shared memory architectures avoiding data race conditions. We demonstrate our approach on actual geophysical applications.

## 1 Introduction

Numerical models are widely used for studying physical phenomena. Most of the time, models are used to forecast or simulate the evolution of a phenomenon. Since a model is imperfect, discrepancy between its forecast values and the so-called “reality” may be significant due to model parametrizations, numerical

discretization, and uncertainties on initial and boundary conditions. Observations, either in-situ or remote-sensing using radars or satellite, give an accurate measurement of physical variables of interest. However they are not error free, for example due to noise of the sensor measurement, and they are in general sparse in time and space.

Data assimilation is a theoretical framework that can blend imperfect knowledge from a numerical model and imperfect measurements from an observational system to give an optimal estimate of control parameters (initial conditions, parameters). In this work we focus in particular on *variational data assimilation* [1], also known as 4D-VAR. This class of methods are widely used in various contexts, e.g. meteorology [2], oceanography [3], and in particular for full three dimensional models. 4D-VAR is based on a minimization with respect to control parameters of a cost function  $J$  which measures the misfit between the direct numerical model outputs and the observations. The minimization is performed using a gradient method, which requires calculating the gradient of  $J$  as a function of the control parameters. The gradient computation requires the product of the transposed Jacobian matrix of the direct numerical model with the derivative vector of  $J$  defined at the observation points. This product is computed through a numerical model, the so-called *adjoint model*. Since the direct numerical model is usually very complex, the implementation of the programming code which represents the adjoint model is often a real issue.

The YAO framework, already presented in [4, 5], is a code generator dedicated to variational data assimilation. With the YAO domain-specific language (DSL), the user defines, using specific directives and C programming, the specifications of the numerical model. It then automatically generates the numerical and the adjoint model codes via C++ object-oriented programming. In practical, if an implementation (e.g. using Fortran or C) of the numerical model already exists, the user may have to recode a non negligible part of the original code. Nevertheless, in the actual YAO applications, it has been noticed that the overhead of the implementation in the YAO formalism is far less than the cost needed to implement the adjoint model from scratch. YAO has already been used with success on several actual applications in oceanography: *Shallow-water* [4, 5], *Marine acoustics* [6, 7], *Ocean color* [8], *PISCES* [9] and the *GYRE* configuration of *NEMO* [10]. YAO is distributed under the free software license CeCILL. Documentation and download are available [11].

Numerical models are based on a discretization of the computational space and apply a number of basic functions at these points. Using YAO the user defines the computational space, the basic functions and their interdependencies. The YAO formalism is based on a dependence graph called a *modular graph*, which is similar to those used in automatic parallelization of nested loops [12]. The traversal of the modular graph allows us to perform all the basic calculations of the numerical model. The user describes, using YAO-specific directives, a traversal of the graph in the form of nested loops, which must be consistent with the different dependencies defined by the modular graph. This task is not trivial for a complex numerical model, thus it is important to check the coherence of the directives defined by the user for a traversal. We present in

this paper an algorithm which allows YAO to automatically check the coherence of a traversal and to detect inconsistencies.

In the field of automatic parallelization of nested loops, several concepts and algorithms have been introduced; these algorithms enable the analysis of nested loops, as well as their decomposition and fusion [12, 13, 14]. The decomposition obtained is well suited to a multi-thread parallelization on shared memory architectures where no communication is required. In this paper, we also show how the YAO modular graph enables us to integrate and adapt these algorithms in order to identify the available parallelism, and to allow the automatic generation of parallel code with YAO while completely avoiding the data race conditions (write/write conflicts). With OpenMP directives, it is then possible to generate a multi-threaded parallel code that runs efficiently on shared memory architectures. This is an important improvement over the previous version of YAO [3], which can generate only sequential code. A large community in geophysics may thus automatically and transparently exploit decades of research in automatic parallelization and benefit from important speedups in computation times on multicore architectures without any additional effort and without any knowledge of parallel programming.

For the automatic generation of parallel code, the development of algorithms specific to YAO is necessary. Indeed, the existing software tools for automatic parallelization with OpenMP directives have specific constraints related to their design, and can therefore currently not be integrated in the YAO generator. For example, the CAPO toolkit [15] supports only Fortran and relies on user interaction to improve the parallelization process. The Gaspard2 framework [16] enables automatic OpenMP code generation, but the available parallelism must first be specified by the user in a UML model. The PLuTo tool [17] can efficiently parallelize nested loops while taking into account, via tiling, data locality on multicore architectures with complex hierarchical memory. However PLuTo does not currently support object-oriented programming for input source codes and it has specific limitations, e.g. only SCoP programs with pure function calls, no dynamic branch conditions, which also prevent a direct integration into YAO. Finally and most importantly, as detailed below there are data race conditions (write/write conflicts) in the generated code. These data race conditions prevent any automatic parallelization from such tools according to their own data-dependency analysis. To our knowledge, none of these tools can automatically insert, for example, OpenMP *atomic* directives to avoid these race conditions and thus enable parallelization. We here show how to efficiently accomplish this in YAO thanks to its modular graph.

Adapting state-of-the-art algorithms to YAO while relying on its modular graph also has several advantages. First, there is no additional constraint on the application code written by the user. Second, a high-level dependency graph is directly provided by the modular graph, which enables us to avoid data-dependency analysis, to naturally obtain a coarse-grain parallelism, and to possibly scale on real-life applications with thousands of statements.

This paper extends a previous work [18] with two additional contributions. First, we introduce a new algorithm, thereafter referred to as the *coherence*

*algorithm*, allowing us to detect inconsistencies in the user-defined YAO modular graph traversal. Second, the coherence and the parallelization algorithms are tested on the European reference model for global oceanography forecasting (*NEMO*, *Nucleus for European Modelling of the Ocean*), which demonstrates that the proposed framework and algorithms are already operational.

In the following section, we will give a brief overview of the YAO framework. Section 3 introduces the coherence algorithm. Then, in section 4, we will show how the modular graph can be used to automatically and efficiently parallelize the generated code on shared memory architectures. Performance results for three actual YAO applications on a multicore CPU are detailed in section 5, including the NEMO application. Finally, in section 6 concluding remarks are presented and future work is discussed.

## 2 YAO overview

### 2.1 The modular graph

We present here the concept of a modular graph, which is fundamental in YAO, as well as the *forward* and *backward* procedures: more details can be found in [4, 5]. We first define the following terms:

- A *module* is an entity of computation; it receives inputs from other modules or from an external context<sup>1</sup> and it transmits outputs to other modules or to an external context.
- A *connection* is a transmission of data from a module to another or between a module and an external context.
- A *modular graph* is a data-flow graph composed of a set of several interconnected modules; it summarizes the sequential order of the computations.

In order to perform data assimilation, at each time step a modular graph is traversed by the *forward* procedure and then by the *backward* procedure.

#### 2.1.1 The *forward* procedure

The input data set of a module  $F_p$  is a vector denoted  $\mathbf{x}_p$  and its output data set is a vector denoted  $\mathbf{y}_p$  (namely  $\mathbf{y}_p = F_p(\mathbf{x}_p)$ ). As a consequence, a module  $F_p$  can be executed only if its input vector  $\mathbf{x}_p$  has already been processed, which implies that all its predecessor modules have been executed beforehand. Thus there are only *flow* dependencies [12] between modules. Since the modular graph is acyclic, it is then possible to find a module ordering, i.e. a topological order, which allows us to correctly propagate the calculation through the graph. If we denote by  $\mathbf{x}$  the vector corresponding to all the graph input data, provided by the external context, the *forward* procedure enables the calculation of the vector

---

<sup>1</sup>An external context is an entity which initializes and retrieves the computation of certain modules.

$\mathbf{y}$  corresponding to all the graph output values. The modular graph defines an overall function  $\Gamma$  and makes it possible to compute  $\mathbf{y} = \Gamma(\mathbf{x})$ . The function  $\Gamma$  has a physical meaning: it represents a direct numerical model  $M$ , with respect to YAO formalism. The *forward* procedure allows us to compute the outputs of the numerical model according to its inputs. The incoming connections from the external context are, for example, initializations or boundary conditions. Outgoing connections transmit their values to compute, as an example, a cost function.

### 2.1.2 The *backward* procedure

This procedure enables the computation of the adjoint of the cost function  $J$  with respect to the control parameters. We suppose that for each module  $F_p$ , with an input vector  $\mathbf{x}_p$  and receiving in its *output data points* a “perturbation” vector  $\mathbf{dy}_p$ , we can compute the matrix product  $\mathbf{dx}_p = \mathbf{F}_p^T \mathbf{dy}_p$ , where  $\mathbf{F}_p^T$  is the transposed Jacobian matrix of the module  $F_p$  calculated at point  $\mathbf{x}_p$ . It is possible [5] to compute the gradient of  $J$  with respect to the control parameters by traversing the modular graph in a reverse topological order and executing local computations on each module in order to compute  $\mathbf{dx}_p$ . Given that an output of a module may transmit its data to multiple entries for other modules, it has been shown [4, 5] that this reversed traversal leads to a back propagation on the modular graph characterized by additions (i.e. accumulations) of several local computations. Each of these additions is computed in an intermediate step and then back propagated. Thus there are here *flow* and *output* dependencies [12].

### 2.1.3 YAO formalism

Running simulations or data assimilations using an operational numerical model  $M$  requires the definition of a modular graph representing the sequence of the computations. A numerical model operates on a discrete grid, where the physical process is computed at each grid point  $\mathbf{I}$  and at each time step  $t$ . As the same phenomenon is under study at each grid point, only the modular subgraph representing a grid point is needed. YAO obtains  $\Gamma$  by duplicating this subgraph for each  $\mathbf{I}$  and  $t$ .

If several scales (in space and times) are present in the numerical model, YAO allows to duplicate some subgraphs for different space and time schemes. In the following, only one space/time trajectory is considered to simplify the notations.

In YAO formalism, the user must define a set of basic functions  $\{F_1, F_2, \dots, F_k\}$  which has to be applied to each grid point  $\mathbf{I}$  and at each time step  $t$ . The user also has to define the dependencies between these functions. From this information, YAO generates the overall modular graph  $\Gamma$ . The modules of the modular subgraph  $\Gamma_{I,t}$  are denoted by  $F_p(\mathbf{I}, t)$ , where  $\mathbf{I}$  represents a grid point (1D, 2D or 3D),  $t$  is a time step and  $F_p$  a basic function. Thus, a module is the computation of the function  $F_p$  at grid point  $\mathbf{I}$  and at time  $t$ . We denote

by  $i$  ( $j$  and  $k$ ) the indices of the first axis (respectively of the second and third axis). An edge from a source module  $F_s(\mathbf{I}', t')$  to a destination module  $F_d(\mathbf{I}, t)$  corresponds to a data transmission from  $F_s(\mathbf{I}', t')$  to  $F_d(\mathbf{I}, t)$  ( $s$  may be equal to  $d$ ).

The modular graph is similar to the Expanded Dependence Graph (EDG) used for the parallelism detection in nested loops [12]. The main difference with the modular graph is in the EDG the nodes represent one operation (the instance of a statement), whereas the nodes of the modular graph are a set of operations (the instance of a function composed by a set of statements) represented by the module  $F_p(\mathbf{I}, t)$ . Thus, the granularity of the nodes differs. In practice the dimension of a YAO basic function depends on the application and on the user design. In general, a YAO module has dozens of statements but in particular cases it may be much larger.

## 2.2 User specifications and code generation

This section presents two YAO directives, *ctin* and *order*. YAO automatic code generation relies on these two directives, which are part of the YAO DSL and allow us to traverse the modules  $F_p(\mathbf{I}, t)$ .

### 2.2.1 *order* and *ctin* directives

The *ctin* directive has the following syntax: “**ctin from**  $F_s$  **to**  $F_d$  *list of coordinates*”. Such a directive represents one edge (or connection) of the modular graph, which is then automatically replicated by YAO in space and time. *list of coordinates* represents, for a generic point  $\mathbf{I}$  and time step  $t$  of the destination module  $F_d$ , the point  $\mathbf{I}'$  and the time  $t'$  of the source module  $F_s$  (with  $t \geq t'$ ). If  $S'$  and  $S$  are the spaces associated to  $F_s$  and  $F_d$  respectively, we denote with  $L'$  and  $L$  the set of axes of  $S'$  and  $S$ ;<sup>2</sup> YAO allows  $S'$  to be a subspace of  $S$  but not  $S$  to be a subspace of  $S'$ , meaning that  $L' \subset L$ . We denote with  $(\mathbf{I}, t)$  the current position of  $F_d$ , with  $(\mathbf{I}', t')$  the relative position corresponding to  $F_s$  and with  $\mathbf{d}$  the distance vector defined by  $\mathbf{d} = \mathbf{I}' - \hat{\mathbf{I}}$ , where  $\hat{\mathbf{I}}$  is the projection of  $\mathbf{I}$  on the axes of  $L'$ . Thus,  $\mathbf{d}$  has the same dimension of  $\mathbf{I}'$ .<sup>3</sup> We denote with  $d_l \in \mathbb{Z}$  its component on the  $l$  axis and with  $d_t = t' - t$  ( $\leq 0$ ) the delay between the time steps  $t'$  and  $t$ . The user has to specify in the *list of coordinates* the distance vector and  $d_t$  as a function of the generic point  $\mathbf{I}$  of the destination module, which is the same in all connections. Figure 1a gives an example of *ctin* directives.

Every *ctin* directive generates an edge from  $F_s$  to  $F_d$  labeled by the distance vector  $\mathbf{d}$  and  $t' - t$ . The resulting graph is a directed multigraph<sup>4</sup> which

<sup>2</sup>The iteration vector  $\mathbf{I}$  can be defined on one ( $\mathbf{I} = (i)$ ), two ( $\mathbf{I} = (i, j)$ ) or three dimensions ( $\mathbf{I} = (i, j, k)$ ) as a function of the space. Likewise for the vector  $\mathbf{I}'$  which is  $\mathbf{I}' = (i + d_i)$ ,  $\mathbf{I}' = (i + d_i, j + d_j)$  or  $\mathbf{I}' = (i + d_i, j + d_j, k + d_k)$  as a function of the space  $S'$ .

<sup>3</sup>The distance vector  $\mathbf{d}$  has a dimension which corresponds to the number of common components between  $S$  and  $S'$ . As an example, if  $S'$  is 2D and  $S$  is 3D the distance vector is 2D and is equal to  $(d_i, d_j)$ .

<sup>4</sup>A directed multigraph is a graph with multiple parallel edges.

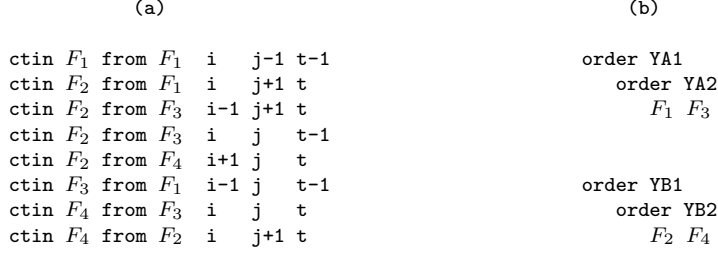


Figure 1: (a) Part of the DSL used by the user with 2D space modules. The second *ctin* directive specifies the connection from  $F_1$  at point  $(i, j+1, t)$  to  $F_2$  at point  $(i, j, t)$ . (b) The *order* directives indicate the ordering in which we compute the  $F_p$  functions and the ordering of the grid traversal.

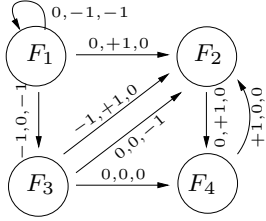


Figure 2: RDG issued by the *ctin* directives of Fig. 1a.

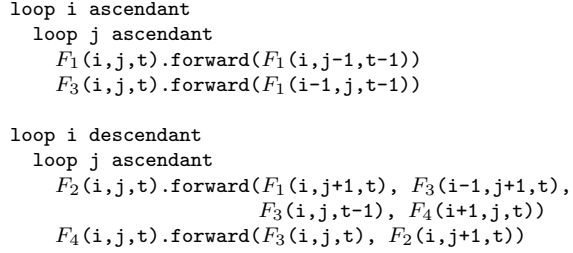


Figure 3: YAO generator translation of the directives of Figs. 1a and 1b.

represents all the dependencies between the basic functions. This multigraph corresponds to the Reduced Dependence Graph (RDG) [12] used for the automatic generation of parallelism in nested loops<sup>5</sup>. Figure 2 presents the RDG of the former example.

Since the space dimension is two, the edges are labeled by  $(d_i, d_j, d_t)$  which indicates that the destination module at time  $t$  and at point  $(i, j)$  takes its inputs from the source module at time  $t + d_t$  and point  $(i + d_i, j + d_j)$  with  $d_i, d_j \in \mathbb{Z}$  and  $d_t \in \mathbb{Z}_{\leq 0}$ .

The YAO *order* directive allows the user to define a traversal of the modular graph following a topological order. This directive allows us to visit all the grid points of the space, and enables the generation of the corresponding nested loops. The user specifies one *order* directive for each dimension of the space. Thus, a program generated by YAO contains an outermost loop representing the time. Within this loop the user defines, thanks to the *order* directives,

<sup>5</sup>As for the analogy between the EDG and the modular graph, the RDG has one statement per node while YAO RDG has a basic function (a set of statements) per node.



the different loops that allow the traversal of the space for each time step. In general, we have several ways to traverse a space. In the *order* directive, *YA1* (YAO Afterward axis 1) means that we are managing the  $i$  loop and we go along this axis in an ascendant way. *YA2* means the same but for the  $j$  axis, whereas *YB1* (YAO Backward axis 1) means that we go along the  $i$  axis in a descendant way. Fig. 1b gives an example of such *order* directives.

### 2.2.2 Generation of the *forward* and *backward* procedures

In Fig. 3 we give the translation, performed by the YAO code generator, of the *ctin* and *order* directives given in Figs. 1a and 1b. This represents the translation, in a pseudo code language, of the *forward* procedure. Each *order* directive generates one loop, one for each dimension of the space. The way we traverse the axes, ascendant or descendant, and the scheduling of the modules are both specified in the *order* directives. For each object of each  $F_p$  module C++ class the local *forward* function (a C++ method) is called using the output of its predecessor modules as inputs. For each basic function, the body of the local *forward* functions are defined by the user. It has to be noticed that all *forward* functions are thread-safe because they compute their results with respect to the generic grid point  $\mathbf{I}$ , as shown in Fig. 3. The nested loops allow us to compute the output of the modules for all the grid points and for one time step. An overall loop, not shown in the figure, which allows us to traverse the time steps in an incremental order  $t, t + 1, t + 2$  etc., encompasses all the local *forward* functions. The time loop may be considered as a computation barrier where at current time  $t$ , all the computations for time  $t' < t$  are done.

As presented in section 2.1.2, the *backward* procedure traverses the modular graph in a reverse topological order. For ease of presentation we do not detail the pseudo code of the *backward* procedure since this one is very similar to the *forward* procedure one. However it is important to point out the addition (accumulation) in the back propagation, detailed in [4, 5] and specific to the *backward* procedure. This accumulation results in *output* dependencies which occur between two time steps. This computation is briefly explained in Fig. 4, which is a partial graph example. The  $y_p$  variables ( $p \in 1, 2, 3$ ) are the outputs of the local *forward* functions. The propagation allows YAO to provide the predecessor module computations to the successor modules. On the other hand, the back propagation allows us to back propagate the gradient of  $J$  by using the Jacobian matrix ( $J_p$  in the figure) for computing  $dx_p$ . The back propagation of several  $dx_p$  ( $dx_3$  and  $dx_2$  in Fig. 4) which have the same predecessor enforces the addition of the  $dx_p$  (the symbol  $\sum$  in the figure).

## 3 Coherence in the computational ordering

The *ctin* and the *order* directives are the basis of YAO DSL. Sometimes the traversal defined using *order* directives can be difficult and in real-world YAO applications the user can make some mistakes in the definition of such an or-

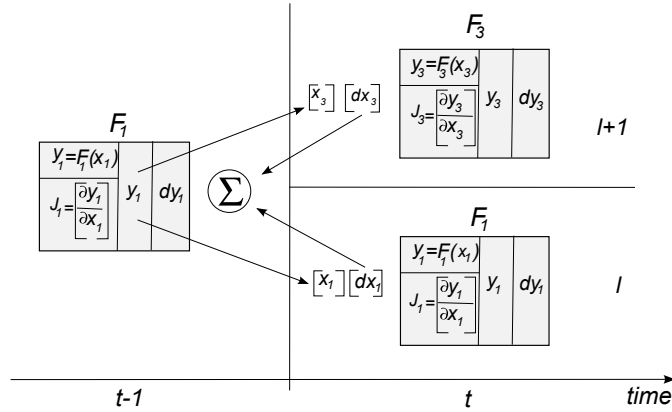


Figure 4: Addition, represented by the symbol  $\Sigma$ , in the back propagation of the *backward* procedure. These two connections represent a data transfer between two time steps. The two modules  $F_3$  and  $F_1$  perform the transfer towards  $F_1$  at time step  $t - 1$ . This partial graph example case is given by the YAO directives shown in Fig. 1.

dering. Defining a wrong traversal implies that when YAO schedules a module for computation its inputs are not ready because its predecessors have not been computed yet. These mistakes directly affect the numerical results of the data assimilation process.

The coherence of a *ctin* directive is defined as follows.

**Definition 1** Assume that  $F_s(\mathbf{I}', t') \rightarrow F_d(\mathbf{I}, t)$  represents a *ctin* directive. This *ctin* is said to be coherent if, for each  $(\mathbf{I}, t)$ , the order directives ensures that the basic function  $F_s$  has already been computed at  $(\mathbf{I}', t')$ . The connection is said to be incoherent otherwise.

In this section we present the rules which allow us to test the coherence of a *ctin* directive. The case where two basic functions  $F_s$  and  $F_d$  are computed at the same time step ( $t = t'$ ) from two different outermost loops (i.e. from two different nests of *order* directives), with respect to the  $L'$  axes, represents the most simple case:

**Rule 1** Assume that  $F_s(\mathbf{I}', t') \rightarrow F_d(\mathbf{I}, t)$ , with  $t' = t$ , is a connection between the basic functions  $F_s$  and  $F_d$ . We suppose that  $F_s$  and  $F_d$  belong to two different outermost loops. If the outermost loop containing  $F_s$  is written before the outermost loop containing  $F_d$ , then the *ctin* directive is coherent otherwise the *ctin* directive is incoherent.

The coherence verification is more difficult as soon as the two basic functions  $F_s$  and  $F_d$  are in the same outermost loop. Given a set of *order* directives, we introduce in section 3.1 two rules to determine the coherence of a *ctin* directive. Then, in section 3.2 we present a general verification algorithm.

### 3.1 Verification rules

**Rule 2** Assume that  $F_s(\mathbf{I}', t') \rightarrow F_d(\mathbf{I}, t)$  is a connection between two basic functions contained in an outermost loop  $l \in L' \cup \{t\}$ , with distance  $d_l \neq 0$ .<sup>6</sup> If  $d_l < 0$  ( $d_l > 0$ ) and the loop  $l$  is ascendant (respectively descendant), then this connection is coherent. In the same way, if  $d_l < 0$  (respectively  $d_l > 0$ ) and the loop  $l$  is descendant (respectively ascendant), then this connection is incoherent.

**Justification** Suppose the loop  $l$  is ascendant. Consider a point  $P = (\mathbf{I}, t)$  with  $I \in S$  and suppose  $l_P$  its component relative to the  $l$  loop. Suppose also  $l_{P'}$  the component relative to the  $l$  loop for the point  $P' = (\mathbf{I}', t')$  with  $I' \in S'$ . If  $l$  is the outermost loop then, at the moment of the computation of  $\mathbf{P}$ , all the points with  $l_{P'} < l_P$  have already been computed due to the ascendant direction of the loop. In fact, when the nested loops compute the iteration  $l_P$ , all the instructions which correspond to an iteration vector  $\mathbf{P}'$  with a component  $l_{P'}$  lower than  $l_P$  have already been computed by the loop  $l$ . If  $d_l < 0$ , then the iteration vector  $\mathbf{P}'$  has  $l_{P'} = l_P + d_l < l_P$  which demonstrates the coherence of the connection. As a consequence if  $d_l > 0$ , then module  $F_s(\mathbf{P}')$  has not been computed yet and the connection is incoherent. The case of a descendant loop is similarly justified.

**Remark 1** Given that the outermost loop concerns the temporal trajectory, rule 2 points out that if  $d_t = t' - t < 0$  then the *ctin* directive is coherent for any set of *order* directives. The verification process must start by testing the coherence with respect to this outermost loop (time). As in YAO the time loop is always ascendant and the delays  $d_t \leq 0$  if a *ctin* directive has  $d_t \neq 0$  then the coherence condition always holds. For ease of presentation if we refer to  $F_s(\mathbf{I})$  we suppose that the time step is  $t$ .

Figure 5a illustrates a traversal on a 2D space, where basic functions A and B are defined. The point  $(i, j)$ , circled in the figure, refers to the current computation point. The grid points computed in the previous iterations are colored in grey. The arrows are all coherent connections with respect to this specific nested *order* directives. These are the connections  $F_s(i-1, j+1) \rightarrow F_d(\mathbf{I})$ ,  $F_s(i-1, j) \rightarrow F_d(\mathbf{I})$ ,  $F_s(i-1, j-1) \rightarrow F_d(\mathbf{I})$ . The three elements which ensure a coherent computation are the outermost loop (the  $i$  axis), the direction YA1 (ascendant) and the sign (-) of  $d_i$ , as shown by rule 2. Note that  $F_s$  and  $F_d$  may be indistinctly A or B.<sup>7</sup> Figure 5b illustrates another example of a 2D traversal with a descendant outermost loop  $j$ ; the arrows are all incoherent connections.

**Rule 3** Assume that  $F_s(\mathbf{I}', t') \rightarrow F_d(\mathbf{I}, t)$  is a connection between two basic functions contained in an outermost loop  $l \in L' \cup \{t\}$ , with distance  $d_l = 0$ . In order to test the coherence we have to remove the outermost loop and keep the

<sup>6</sup> $L'$  is the set of axes of the space  $S'$ .

<sup>7</sup> $A(i-1, j+1) \rightarrow A(\mathbf{I})$ ,  $B(i-1, j) \rightarrow A(\mathbf{I})$  and  $B(i-1, j-1) \rightarrow B(\mathbf{I})$  are also coherent connections.

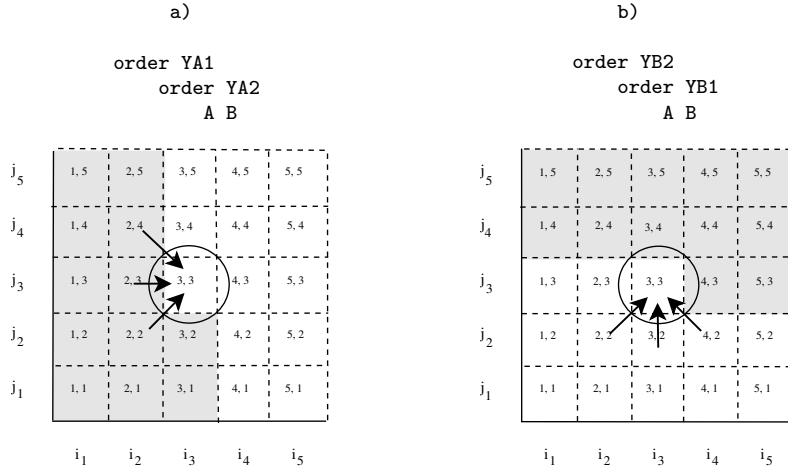


Figure 5: Traversal given by two nested *order* directives on a  $5 \times 5$  space. Grid point  $\mathbf{I} = (i, j) = (3, 3)$  is the current iteration point. The grey and white squares represent the computed and not yet computed grid points respectively. The arrows represent coherent connections (a) and incoherent connections (b).

*rest of its instructions (loops and basic functions). We may have two cases for the remaining instructions:*

- $F_s$  and  $F_d$  are in the same embedded loop: we apply rule 2 or rule 3 recursively.
- $F_s$  and  $F_d$  are in two different instructions: we apply rule 1.

**Justification** In case  $d_l = 0$ , the basic functions  $F_s$  and  $F_d$  are computed in the same iteration of the loop computing the  $l$  axis. This loop computes one or several instructions which represent the computation of either a basic function or a loop (nested in the former  $l$  loop). Thus, if the basic functions  $F_s$  and  $F_d$  are computed with the same loop nested in  $l$ , then we must verify the coherence with respect to this inner loop, for this reason we must apply either rule 2 or 3. However, if the basic functions  $F_s$  and  $F_d$  are computed by two different instructions in the  $l$  loop, rule 1 is applied, i.e. the instruction containing  $F_s$  must be computed before the one containing  $F_d$ .

**Example 1** Test the coherence of connection  $A(i, j + d_j, t) \rightarrow B(\mathbf{I}, t)$ , with  $d_j \in \{-1, 0, +1\}$ , given the *order* directives on the left side:

<pre> order YA1   order YA2     A   order YB2     B </pre>	<pre> order YB2   A order YB2   B </pre>
--	--

We apply rule 3. After removing the outermost loop on  $t$  and then the one on  $i$

```

order YA1
  A
  order YA2
    B C
  order YA2
    order YA1
      D
    order YB3
      E

```

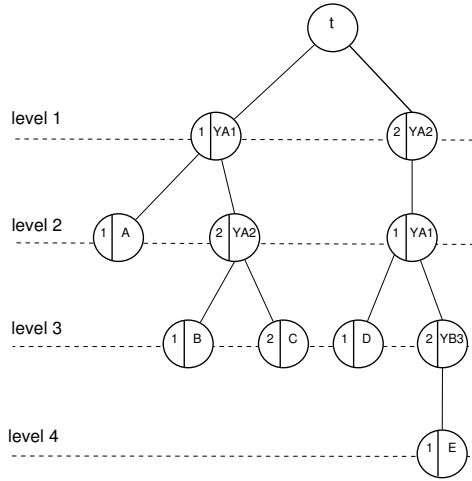


Figure 6: Example of *order* directives defined by the user. The basic function  $E$  is applied to a three dimension space, whereas  $B, C, D$  and  $A$  are applied to two and one dimension spaces respectively.

Figure 7: Tree representation of the *order* directives of Fig. 6. Leafs and internal nodes represent basic functions and loops respectively. They are characterized by  $YXl$  ( $X \in \{A, B\}$ ,  $l \in \{1, 2, 3\}$ ) and *child\_number*.

we obtain the directives on the right side. Since  $A$  and  $B$  are contained in two different outermost loops and since  $A$  precedes  $B$ , the connection is coherent (rule 1).

### 3.2 Coherence algorithm

The overall verification process is given by testing the coherence of each *ctin* directive. The algorithm parses each connection independently. Taking into account remark 1, we know that every *ctin* directive which verifies  $d_t \neq 0$  is coherent. Thus we limit the coherence process to the verification of the *ctin* directives which verify  $d_t = 0$ . To introduce the coherence algorithm we present in Fig. 6 an example of *order* directives.

In this example the user specifies two nested *order* directives. The *forward* procedure starts with the computation of the nested *orders* containing  $A$ ,  $B$  and  $C$ ; then the second nested *orders*, which contain the basic functions  $D$  and  $E$ , are computed. Each nest of *order* directives is composed of an outermost loop, described by the parameter  $YXl$ , with  $X \in \{A, B\}$  and  $l \in \{1, 2, 3\}$  standing for  $\{i, j, k\}$ . The body of an outermost loop is composed of three types of instruction lists: (i) a list of loops; (ii) a list of basic functions; (iii) a list composed of both loops and basic functions.

As in the compiler theory [19], it is possible to organize the *order* directives

by an Abstract Syntax Tree (AST). Figure 7 shows the tree corresponding to the example of Fig. 6. The root children are the outermost *order* directives (two in the example); these nodes correspond to level 1 (the root being at level 0). In general, each node of the tree corresponds to one instruction. This instruction may be either a loop, corresponding to an *order* directive, or the computation of a basic function. A node which computes a basic function has no children and is represented by a leaf of the tree. A node which corresponds to a loop has as many children as the number of instructions contained in its loop. These children are placed in the successive level with respect to the level of the parent (parent level plus one).

Each internal node (which is not a leaf or the root) represents a loop defined by its axis and its direction. The children of a node are numbered in the ordering of the user declaration. We denote this number as *child\_number*. An internal node of the tree contains also the parameter *YXl*, which specifies the loop axis and the direction. A leaf contains the basic function name.

With this representation if we want to characterize the nested loops which enclose the calculation of a basic function, we only have to determine the path from the root to the leaf which represents the basic function. The internal nodes of this path represent the nested loops which allow the computation of the basic function. If we do not consider the root, the first node of the path corresponds to the outermost loop and the last node corresponds to the basic function. Thus, for each basic function, we can create a list which represents the path with at most three intermediate internal nodes. Each internal node contains the following fields: (i) *child\_number*, ordering from left to right of the children of a parent node; (ii) *axis*, loop index ( $axis \in \{i, j, k\}$ ); (iii) *direction*, ascendant or descendant of the loop. The *axis* and the *direction* are represented in Fig. 7 by the parameter *YXl*. Thanks to the rules introduced in the previous sections and to the tree structure, we can verify the coherence of a particular *ctin* directive using Algorithm 1. We explain the general idea of this algorithm through some examples.

**Example 2** In Fig. 7, we consider a connection  $B(i-1, j) \rightarrow C(i, j)$ , where  $d_i = -1$  and  $d_j = 0$ , and we check its coherence. Figure 8a shows the paths  $P_b$  and  $P_c$  for the basic functions  $B$  and  $C$ : they have three levels ( $n = 3$ ). At the first iteration  $m = 1$ , the *child\_number*, the *axis* and the direction of nodes  $N_s$  and  $N_d$  are 1 and YA1. The conditions of lines 8 and 11 are *false*, we are in the same loop. Since *direction* = *ascendant* and  $d_i < 0$ , rule 2 of line 16 gives that the *ctin* is coherent, the algorithm ends returning *true*.

**Example 3** We now consider a connection  $A(i) \rightarrow B(i, j)$ , and we test its coherence. This is the case of data transfers between computational spaces which have a relation of projection:  $A$  and  $B$  are basic functions applied to 1D and 2D spaces respectively.  $P_s$  and  $P_d$  have two and three levels respectively (Fig. 8b). At iteration  $m = 1$ , the basic functions are in the same loop (the conditions of lines 8 and 11 are *false*) and, since  $d_i = 0$ ,  $m$  is incremented. At iteration  $m = 2$ , the condition at line 8 is *true*, because we have on one hand

---

**ALGORITHM 1:** Coherence verification of a given *ctin* directive with respect to the *order* directives.

---

**Require:** Denote by  $F_s(\mathbf{P}, t') \rightarrow F_d(\mathbf{I}, t)$  the connection which represents the *ctin* directive.  $d_l$  is the distance of the vector  $\mathbf{d} = \mathbf{P} - \hat{\mathbf{I}}$  with respect to the  $l$  axis.

**Ensure:** *true* if the *ctin* is coherent, *false* otherwise.

```

1: if  $d_t < 0$  then
2:   return true
3: end if
4: Find two paths  $P_s$  and  $P_d$  from the root to the leafs  $F_s$  and  $F_d$ .
5: Let  $n$  be the minimum length of  $P_s$  and  $P_d$ .
6: for  $m = 1$  to  $n$  do
7:   Determine at the level  $m$  the two nodes  $N_s$  and  $N_d$  of the tree which are
   located on the two paths  $P_s$  and  $P_d$  respectively.  $\{N_s$  and  $N_d$  are either
   the same or two siblings.}
8:   if child_number of  $N_s <$  child_number of  $N_d$  then
9:     return true
10:  end if
11:  if child_number of  $N_s >$  child_number of  $N_d$  then
12:    return false
13:  end if {At this point the two nodes are identical.}
14:  Assume that  $l$  is the axis corresponding to the common loop.
15:  if  $d_l \neq 0$  then
16:    return the result of rule 2.
17:  end if
18:   $m \leftarrow m + 1$  {Continue to the successive level, i.e. apply rule 3.}
19: end for
20: return false

```

---

the node of the basic function  $A$ , and on the other hand the  $j$  loop containing  $B$ . We test rule 1, i.e. the precedence of  $A$  with respect to  $B$ , which is given by *child\_number* of  $N_s$  and  $N_d$ . The algorithm returns *true*.

### 3.3 Results of the coherence algorithm

The coherence algorithm solves the problem of verifying that a given *ctin* directive is correctly computed using the user-defined graph traversal. This algorithm is applied to each user-defined connection. If all values returned are true we can ensure that *ctin* and *order* directives are written coherently. The coherence algorithm has been implemented and tested on both fictitious and actual YAO applications. It plays an important role during the development of a YAO application with hundreds of *ctin* and *order* directives, enforcing the robustness of the variational data assimilation process. The tests on actual applications have led to the detection of a couple of real incoherences which had never been de-

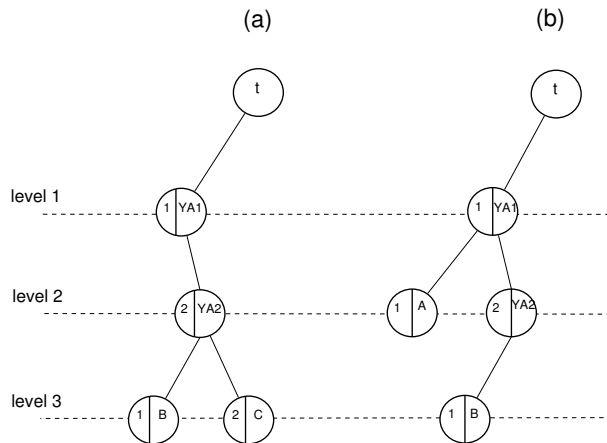


Figure 8: Two examples of path  $P_s$  and  $P_d$  for the tree of Fig. 7 and the basic functions: (a) B and C; (b) A and B.

tected by human observations. The detection of these incoherences has led to an improvement in the precision of the numerical results of these YAO applications.

The next section deals with the automatic parallelization of the *forward* and *backward* procedures based on coherent directives. The coherence algorithm itself is excluded by the parallelization process. Indeed, it does not represent a performance bottleneck, being able to analyze at generation-time thousands of directives in a matter of milliseconds.

## 4 Algorithm for automatic parallelization

### 4.1 Parallelization of the *forward* procedure

In section 2 we have noted an interesting similarity between YAO formalism and the theories of compilation and of automatic parallelization of nested loops [12]. Thanks to this similarity we can adapt these techniques and algorithms to YAO automatic code generator. We thus propose here to integrate and adapt such algorithms in order to automatically parallelize the *forward* procedure generated by YAO on parallel shared memory architectures with multi-thread programming. No communication is required and we only have to maximize the number of parallel loops. Because of the strong time dependencies in all data assimilation applications the temporal loop is not parallelized and we focus on data parallelism at each time step. The domain decomposition between threads is performed as a 1D block distribution on the space and we rely on a static load balancing since in all the current YAO applications the computation load of each module is constant at each grid point. Our goal is thus to label, as “parallel” or “not parallel”, each outermost *order* directive so that the corresponding loop can be generated as parallel or sequential in the final code (thanks to OpenMP



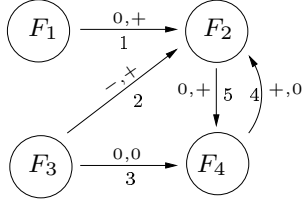


Figure 9:  $\overline{\text{RDG}}$  obtained by simplification of the RDG of Fig. 2. The edges are numbered from 1 to 5.

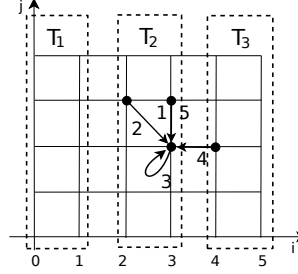


Figure 10: *Flow dependencies* between three threads  $T_1$ ,  $T_2$  and  $T_3$ . Same edge numbers as in Fig. 9.

directives). In order to maintain the coherence hypothesis of one given nest of *order* directives, we opted not to change or invert the *order* defined by the user. However we can still use techniques such as loop distributions possibly followed by loop fusions in order to detect the maximum available parallelism and to reduce the synchronization points.

Since the temporal loop is not considered in the parallelization algorithm the edges whose  $t' - t$  are negative can be removed from the RDG. The remaining graph is shown in Fig. 9: we denote it  $\overline{\text{RDG}}$ . This is obtained by removing all  $dt = -1$  connections and by writing only the signs of the distance vector components. Thus  $(0, +)$  means a distance vector equal to  $(0, +1)$ .

Considering some nested *order* directives which have as outermost axis  $l$  and a connection from  $F_s$  to  $F_d$ , we consider a connection as *critical* with respect to these nested order directives if:

- $F_s$  and  $F_d$  are contained by the nested directives,
- $d_t = 0$  and  $d_l \neq 0$ .

The analysis of the  $\overline{\text{RDG}}$  highlights the critical connections which prevents parallelization because of *flow dependencies* between threads, as presented in Fig. 10. The connections from  $F_4$  to  $F_2$  and from  $F_3$  to  $F_2$  (edges #2 and #4 in Figs. 9 and 10) result in two *flow dependencies* between the couples of threads  $(T_1, T_2)$  and  $(T_2, T_3)$  because  $d_l \neq 0$  (in this example  $l$  is the  $i$  axis). This is not the case for the connections #1, 3 and 5 because the two corresponding grid points belong to the domain computed by one thread, as shown in Fig. 10. The connection #2 is *not critical*, since  $F_3$  and  $F_2$  are not in the same nested loops (see Figs. 1b and 3). Therefore, in this example only the connection #4 is *critical*.

For the analysis of one outermost loop  $l$  composed of functions  $F_1, F_2, \dots, F_r$  we consider the subgraph  $G_l$  of the  $\overline{\text{RDG}}$  limited to the  $r$  basic functions and to the edges between them. On the edges of this subgraph we retain only

information concerning the distance  $d_l$ .<sup>8</sup> As far as the  $d_l$  value is concerned we retain only the sign of  $d_l$ ,  $(-, +)$  if  $d_l \neq 0$  and 0 if  $d_l = 0$ . The analysis of  $G_l$  allows us to decompose the loop into several loops preserving the computation coherence hypothesis. Taking into account that the *forward* functions are thread-safe, we can apply the Allen-Kennedy algorithm [14] to decompose the loop into parallel loops as follows.

- Calculate the Strongly Connected Components (SCCs) of  $G_l$ .
- Consider the reduced Directed Acyclic Graph (DAG), denoted by  $G_{l/SCC}$ , by shrinking each SCC down to a single vertex and by drawing one, and only one, edge between two SCCs if there is at least one edge from the first to the second in the graph  $G_l$ . If at least one of the edge in  $G_l$  which connects these two SCCs is labeled by non 0 (that is to say either  $-$  or  $+$ ), then label the corresponding edge in  $G_{l/SCC}$  by this value. Otherwise, if all the labels are 0, then label the corresponding edge in  $G_{l/SCC}$  by 0.
- Sort in a topological order the  $G_{l/SCC}$  graph and enumerate all the SCCs following this order. For each SCC generate an  $l$  loop which computes its basic functions.

This decomposition is a maximum loop distribution of the initial loop; in other words, we can not further decompose without breaking the coherence hypothesis.

We can analyze each SCC loop in order to see if we can perform a domain decomposition on the  $l$  axis. For a particular SCC we consider all the edges of the graph  $G_l$  between two basic functions being part of this SCC. If at least one of these connections is labeled by  $+$  or  $-$ , namely if  $d_l \neq 0$ , the SCC is considered to be not parallelizable. The loop is parallelizable if all these edges are labeled by 0. In other words it is parallelizable if it does not contain any *flow* dependency between threads. We label by  $p$  and  $\bar{p}$  the loops which are parallelizable and not parallelizable respectively. Such maximum loop distribution gives the largest number of parallel loops. The critical connections of the  $\overline{RDG}$  have been minimized. An example of this algorithm is presented in section 4.4.

## 4.2 Reducing synchronization points

In the previous section, we have applied the Allen-Kennedy algorithm to YAO thanks to the analogies between the EDG and the modular graph. This algorithm enables us to automatically label as parallel or not the SCCs resulting in a maximum loop distribution. With regards to performance, this loop distribution is not the best solution because it increases the number of synchronization points. Following Kennedy-McKinley [13] it is possible to propose a loop fusion algorithm that will reduce the number of synchronization points. As the  $G_{l/SCC}$  is a DAG, we can reorganize the SCCs in levels. The levels are numbered from

<sup>8</sup>All the distances  $d_l$  in  $G_l$  are either  $\leq 0$  if the  $l$  loop is ascendant, or  $\geq 0$  if the  $l$  loop is descendant, as they correspond to the same outermost loop.

---

**ALGORITHM 2:** Fusion with levels approach.

---

```
1: Organize the graph  $G_{I/SCC}$  in  $M_{level}$  levels. The vertices are labeled by either  $p$ 
   or  $\bar{p}$ .
2: Traverse the graph and for each level merge the vertices of the same label.
   Update edges and their labels (0, - or +).
3:  $k := 1$ 
4: while  $k < M_{level}$  do
5:   Consider two consecutive levels  $k$  and  $k + 1$ :
6:   if there are two vertices labeled by  $p$  and there is no critical edge between
   them then
7:     Fusion the two in one vertex labeled by  $p$ 
8:   else
9:     if there are two vertices labeled by  $\bar{p}$  then
10:      Fusion the two in one vertex labeled by  $\bar{p}$ 
11:    end if
12:  end if
13:  if a fusion has been performed then
14:    Reorganize the new reduced graph in levels and update  $M_{level}$ 
15:  else
16:     $k := k + 1$ 
17:  end if
18: end while
```

---

$k = 1$  to  $k = M_{level}$ , where  $M_{level}$  is the maximum number of levels. The first level,  $k = 1$ , contains the SCCs without predecessors; the predecessors of a SCC at level  $k$ , with  $k > 1$ , are located in the preceding levels  $k'$  ( $k' \leq k - 1$ ), with at least one predecessor located at level  $k - 1$ . Because of the level reorganization there is no edge between two vertices at the same level. For each level it is then possible to merge all vertices labeled as  $p$  and separately all vertices labeled as  $\bar{p}$ . We obtain a reduced graph with the same number of levels but with one or two vertices per level. If a level contains two vertices they are mandatory labeled as  $p$  and  $\bar{p}$ .

The fusion process can be extended to the vertices located at two consecutive levels as follows: for all levels  $k$  and  $k + 1$ ,

- merge two vertices labeled as  $\bar{p}$ : this gives a new  $\bar{p}$  vertex;
- merge two vertices labeled as  $p$  which are not connected by a *critical* edge ( $d_l = 0$ ): this gives a new  $p$  vertex.

The fusion process between different levels may modify the vertex level repartition. However the modification can affect only some levels: it does not impact the levels which precede  $k$ . Algorithm 2 allows us to manage the fusion of the vertices with the level technique which maintains the highest degree of parallelization. The final reduced graph is treated by YAO, which generates code according to the following steps.

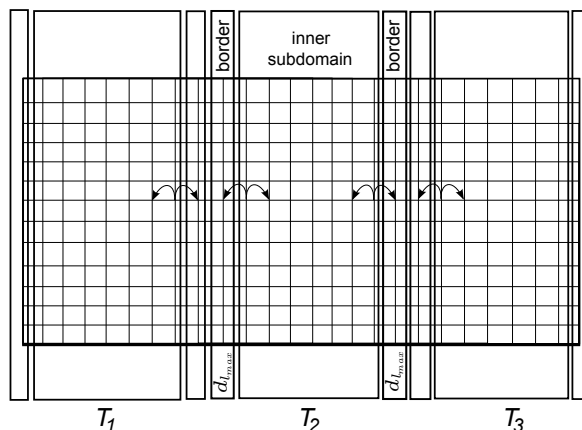


Figure 11: Subdomain decomposition with  $d_{l_{max}} = 1$  for threads  $T_1$ ,  $T_2$  and  $T_3$ . Each thread domain is decomposed into two *border* subdomains with  $d_{l_{max}}$  grid points in the parallel dimension, and one *inner* subdomain.

- Sort in a topological order the final reduced graph and enumerate all its vertices following this topological order.
- Write one nest *order* directives for each vertex. These *order* directives have the same axes as the one provided by the user and contain the basic functions merged in the vertex.
- Generate OpenMP directives for vertices labeled by  $p$ .

An example of this algorithm is presented in section 4.4.

### 4.3 Parallelization of the backward procedure

The same parallelization algorithm can also be applied to the *backward* procedure, which results in a complete parallelization of all computations at each time step. The total elapsed time in a YAO application is mainly composed of the *forward* and the *backward* elapsed times. Parallelizing these two procedures means that most of the application has been optimized. Profiling measurements on some YAO applications showed that 99 percent of the total elapsed time is generally in these procedures.

The RDG used for the *backward* procedure is the same as for the *forward* procedure but the arrows are reversed with respect to the original RDG. These two RDGs have the same SCCs. As the outermost loops also have the same axis, the same method used to parallelize the *forward* procedure is also valid to parallelize the *backward* procedure. Likewise, it is easy to see that the rules used to merge loop blocks previously introduced remain valid for the *backward* procedure. Thus, parallel *order* directives obtained by the decomposition/merging

methods defined for the *forward* procedure can be fully retained for the *backward* procedure.

However the parallelization of the *backward* procedure has a further difficulty in terms of thread synchronization. This synchronization is required by the addition (accumulation) presented in section 2.2.2. As shown in Fig. 4, in a parallel context this addition may result in a data race condition (write/write conflicts) if the back propagations of  $dx_p$  are performed concurrently by several threads. Such conflicts may occur between two time steps. Hence, the analysis of the  $\overline{\text{RDG}}$  is not sufficient to detect all the data race conditions of the *backward* procedure.

This issue can be solved with OpenMP *atomic* directives which ensure that each addition is performed atomically. However these atomic instructions are costly, as well as numerous in the *backward* parallel code, which prevents us from obtaining good parallel performances in practice. In order to avoid these OpenMP *atomic* directives, we rely on the distance vectors of the RDG to determine the maximum  $|d_l|$ , denoted  $d_{l_{max}}$ . In the 1D block decomposition, we can now further decompose each thread domain into three subdomains: two *border* subdomains with  $d_{l_{max}}$  grid points in the parallel dimension, and one *inner* subdomain with usually much more than  $d_{l_{max}}$  grid points in the parallel dimension. An example with  $d_{l_{max}} = 1$  is presented in Fig. 11. Data race conditions are now avoided by ensuring that all threads compute the three subdomains in the same ordering. OpenMP barrier directives are required between each subdomain computation.

Taking all this into account, the overall parallelization algorithm ensures the parallelization of all the computations done by a YAO generated application. It gives a domain decomposition with respect to the outermost loop  $l$ , which can then be automatically parallelized in the final generated code thanks to OpenMP directives. Furthermore if a multi-level parallelization is desired, it is then possible to apply the same algorithm for each subloop. We emphasize that the parallel code generated by YAO respects the *order* and the *ctin* directives, which implies that the result of the parallel code is the same as the sequential code.

#### 4.4 Marine acoustics example

This section presents an example of the decomposition algorithm on a 2D modular graph taken from an actual YAO application. The Marine acoustics example has a small number of functions  $F_i$ , which allows us to easily show the evolution of the RDG graph. We use the same function names as [7, 6]. This YAO application deals with marine acoustics and allows us to assimilate actual observations of acoustic pressure in order to retrieve some geoacoustic parameters like celerity, density and attenuation. In [7] the basic functions are denoted by  $n(z)$ ,  $C$ ,  $B$ ,  $bet$ ,  $gam$ ,  $R$ ,  $X_t$ ,  $\psi$  and  $\psi_{fd}$ . To make it simpler we denote them by  $F_1, \dots, F_9$  respectively. Figure 12 shows the *RDG* composed of  $r=9$  basic functions and the edges labeled with the coefficient signs of the *ctin* directives. In this figure the SCCs are outlined by the dashed lines and numbered from 1 to 6.

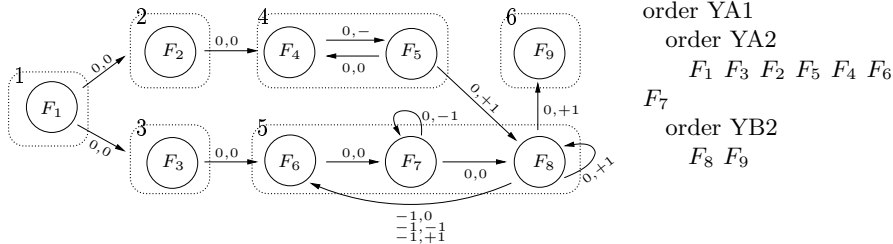


Figure 12: RDG: the dashed lines are the Strongly Connected Components.

order YA1  
order YA2  
 $F_1 F_3 F_2 F_5 F_4 F_6$   
 $F_7$   
order YB2  
 $F_8 F_9$

Figure 13: *order* directives defined by the user for the Marine acoustics example.

The *order* directives specified by the user are given in Fig. 13. In this case, the outermost loop is related to the ascendant  $i$  axis. After computing the  $G_{I/SCC}$  graph, we label each vertex and we proceed with the level reorganization, as presented in Fig. 14, where  $M_{level}$  equals 5; the single circle denotes a parallelizable vertex ( $p$ ) and the double circle a non parallelizable vertex ( $\bar{p}$ ). Fig. 16 shows the fusion of the vertices 2 and 3 labeled by  $p$  in a new vertex called 2,3 of the same label. This is done in the initialization phase of the algorithm (line 2). Then the vertices 1 and 2,3 can be merged in a new vertex called 1,2,3 which is parallel too. The two vertices are located on levels  $k = 1$  and  $k = 2$ . A level reorganization reduces  $M_{level}$  to 4. The same operation is done on the vertices 1,2,3 and 4, followed again by a level reorganization ( $M_{level}$  reduced to 3). The topological order is then: [1,2,3,4], [5], [6] as shown in Fig. 17. The algorithm ends because it is no longer able to fuse and the level counter has reached  $M_{level}$  equals 3. This topological order is translated in an ordering of the modules. The final scheduling respects the ordering given by the user and corresponds to:  $[F_1 F_3 F_2 F_5 F_4]$ ,  $[F_6 F_7 F_8]$ ,  $[F_9]$  or  $[n(z) B C gam bet]$ ,  $[R X_t \psi]$ ,  $[\psi_{fd}]$ . The final decomposition of the *order* directives is in Fig. 15. With the keywords *parallel* and *non parallel* this figure outlines the outermost loops (*order* directives) that the algorithm has recognised as parallel or not.

## 5 Performance results

We present the performance results of the parallel code generated by YAO (changelist 613 [11]) for both simple and complex actual applications of data assimilation. Experiments are performed on a server at Polytech Paris-UPMC (France), composed of one AMD Magny-Cours Opteron 6168 processor and 16 GB of memory. This processor has 12 cores running at 1.9 GHz which have private L1/L2 (64KB/512KB) caches and share two 6MB L3 caches. All computations are performed in double precision.

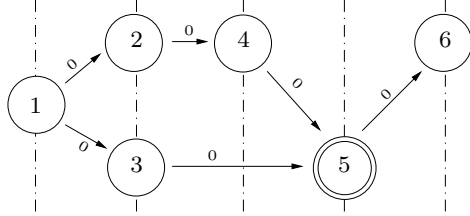


Figure 14:  $G_{I/SCC}$  where the double circle represents a non parallelizable vertex.

order YA1 (**parallel**)  
 order YA2  
 $F_1 F_3 F_2 F_5 F_4$

order YA1 (**non parallel**)  
 order YA2  
 $F_6 F_7$   
 order YB2  
 $F_8$

order YA1 (**parallel**)  
 order YA2  
 $F_9$

Figure 15: *order* directives recomputed by the algorithm for the Marine acoustics example.

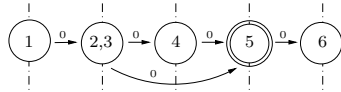


Figure 16: Fusion of the vertices 2 and 3 in a new  $p$  vertex called 2,3.

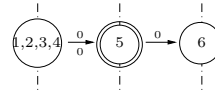


Figure 17: Fusion of the vertices 1,2,3 and 4 in a new  $p$  vertex called 1,2,3,4.

## 5.1 Simple data assimilation applications

We focus here on two simple, but actual, data assimilation applications: the Shallow-water and the Marine acoustics applications mentioned before.

The RDG of the Shallow-water application is composed of 6 SCC (each SCC contains one basic function), see [4, 5] for more details. The parallelization algorithm returns that all SCCs are parallelizable. Figure 18 shows the elapsed times and the parallel speedups for an increasing number of cores used (with one OpenMP thread per core) and for different computational space sizes, with both OpenMP *atomic* directives and our subdomain decomposition. The data race conditions in the *backward* procedure are more efficiently avoided with our subdomain decomposition which clearly offers better performance than the *atomic* directives. We emphasize that such OpenMP code automatically generated by YAO is equivalent to a (non-trivial) manual parallelization, and offers good speedups (up to 9.4 on 12 cores). Moreover for a fixed number of cores the speedup increases with the computational space size since this increases the computation grain of each thread.

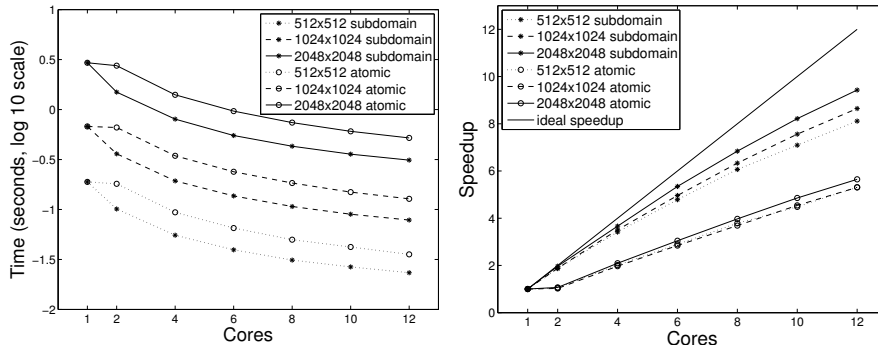


Figure 18: Shallow-water performance measurements for three 2D computational space sizes over one time step (time averaged over 30 time steps). Both performance results with OpenMP *atomic* directives and subdomain optimization are shown. The times encompass both the *forward* and the *backward* procedures.

The performance results on the Marine acoustics are very different. In section 4.4 we have shown that the parallelization algorithm does not parallelize the whole RDG. Three modules, which unfortunately contain most of the computation, are excluded from the parallel region. Figure 19 shows the elapsed times and the parallel speedups, as well as the theoretical maximum speedup according to Amdahl’s law for this application. The parallel speedup is very limited, but the code generated by YAO offers most of the speedup available in this application. Again, the performance gain increases with the computational space size.

## 5.2 A complex data assimilation application

We now focus on the much more complex NEMO application, which requires a greater number of modules. NEMO [10] is a state-of-the-art complete three-dimensional ocean modeling framework based on the finite difference approximation of Navier-Stokes equations. NEMO is used by a large community: 240 projects in 27 countries (14 in Europe, 13 elsewhere) and its evolution and reliability is controlled by an European consortium<sup>9</sup>. The GYRE configuration of NEMO is considered in this work. In this configuration, the dimension of the computational space is fixed at  $32 \times 22 \times 31$  for each time step. The YAO implementation of this numerical model involves 82 modules that are computed within 11 nested loops. Among these 11 loops, 2 loops (containing 1 module each) are excluded from the parallel region and represent 2.1% of the serial execution time. 80 out of the 82 modules are thus parallelized by YAO. Due to the limited dimensions of the computational space of the GYRE configuration,

<sup>9</sup><http://www.nemo-ocean.eu/>



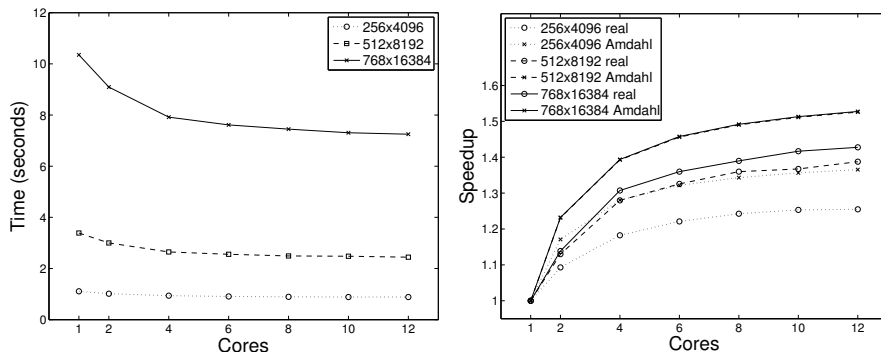


Figure 19: Marine acoustics performance measurements for three 2D computational space sizes over one time step (time averaged over 30 time steps). The times encompass both the *forward* and the *backward* procedures.

parallel performance tests were performed only up to 8 cores. We use here our subdomain decomposition in order to obtain the best parallel speedups.

Figure 20 shows the elapsed times and the parallel speedups, as well as the theoretical maximum speedup according to Amdahl’s law for this NEMO application, as generated by YAO with OpenMP. Thanks to YAO, we automatically obtain good parallel speedups: up to 5.71 on 8 cores. According to Amdahl’s law, this represents 81.8% of the maximum theoretical speedup (namely 6.98) available on 8 cores for this complex and actual data assimilation application.

## 6 Conclusion and perspectives

In this paper we have shown how the modular graph formalism of YAO allows us to address some important automatic generation tasks. During the development of a new YAO application the writing of the *order* directives is a costly phase. The coherence algorithm allows the user to speed up this development. We have highlighted some rules which may in the future open the way to a completely automatic generation of the *order* directives. Moreover, the user-defined *order* directives are important from a performance point of view. The automatic generation of *order* directives may allow nested loops which minimize the computation time by exploiting at best the CPU memory hierarchy. This is a subject under study.

We have also shown how the modular graph allows us to address the issue of the automatic parallelization of the code generated by YAO. Indeed, a YAO modular graph is generated by a reduced graph, which is similar to the Reduced Dependence Graph (RDG) used in the automatic parallelization of nested loops. This similarity allows the adaptation to YAO of the algorithms that were developed in this research field. We have thus presented here how the Allen-Kennedy [14] and Kennedy-McKinley [13] algorithms can be integrated and adapted in

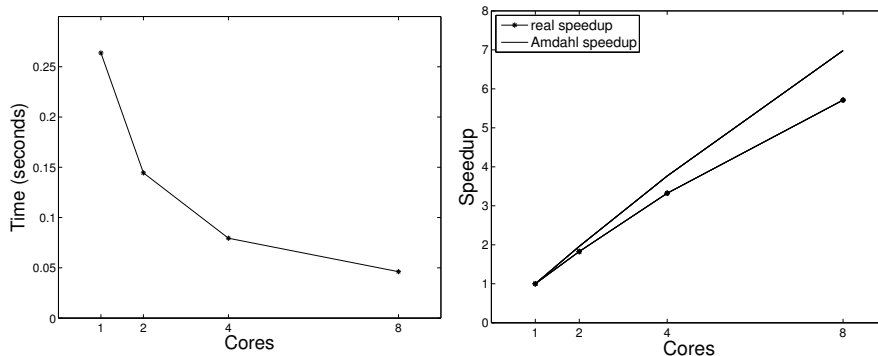


Figure 20: NEMO performance measurements over one time step (time averaged over 30 time steps). The times encompass both the *forward* and the *backward* procedures.

order to enable the automatic parallelization, via multiple threads on parallel shared memory architectures, of the application code generated by YAO. In the *backward* procedure the modular graph is furthermore used to decompose each thread domain into three subdomains, whose appropriate sizes enable us to completely avoid the race conditions occurring in this *backward* procedure. We have also presented performance results of the parallel generated code with OpenMP on a multicore CPU for both simple (Shallow-water, Marine acoustics) and complex (NEMO) actual applications. We automatically obtain good speedups for these applications with up to around 80% of parallel efficiency on 8 or 12 CPU cores, within the limits of the parallelism available in each application.

More advanced transformations (unimodular transformation, loop inversion, SIMD vectorization, tiling, ...) have already been developed in the context of automatic loop parallelization, especially via the *polyhedral model* [12, 17]. We are currently studying if and how this polyhedral model can be integrated in the YAO framework. In the future, we also plan to investigate the automatic generation of MPI code from OpenMP code in the YAO context in order to automatically scale data assimilation applications on distributed memory architectures. It can be noticed that the subdomain decomposition between border and inner subdomains, presented here to avoid race conditions, may help overlap MPI communications with computation in order to obtain the best speedups in a distributed memory context: here again, the modular graph of YAO may be very useful to automatically determine this subdomain decomposition for any variational data assimilation application. Finally, these automatically inserted OpenMP directives could also be rewritten as OpenACC<sup>10</sup> directives in order to automatically generate parallel code for GPUs (Graphics Processing Units).

<sup>10</sup>Open industry standard of compiler directives for accelerators, see: <http://www.openacc-standard.org/>

## References

- [1] O. Talagrand. Assimilation of Observations, an Introduction. *J. Meteor. Soc. Japan*, 75:191–209, 1997.
- [2] AM Clayton, Andrew C Lorenc, and Dale M Barker. Operational implementation of a hybrid ensemble/4d-var global data assimilation system at the met office. *Quarterly Journal of the Royal Meteorological Society*, 139(675):1445–1461, 2013.
- [3] Hans Ngodock and Matthew Carrier. A 4dvar system for the navy coastal ocean model. part i: System description and assimilation of synthetic observations in monterey bay\*. *Monthly Weather Review*, 142(6):2085–2107, 2014.
- [4] L. Nardi, C. Sorrow, F. Badran, and S. Thiria. YAO: A Software for Variational Data Assimilation Using Numerical Models. In *LNCS 5593, Computational Science and Its Applications (ICCSA)*, pages 621–636, 2009.
- [5] L. Nardi. *Formalisation et automatisation de YAO, générateur de code pour l’assimilation variationnelle de données*. Ph.D. thesis, CNAM, 2011.
- [6] F. Badran, M. Berrada, J. Brajard, M. Crépon, C. Sorrow, S. Thiria, J.-P. Hermand, M. Meyer, L. Perichon, and M. Asch. Inversion of Satellite Ocean Colour Imagery and Geoacoustic Characterization of Seabed Properties: Variational Data Inversion Using a Semi-automatic Adjoint Approach. *J. of Marine Systems*, 69:126–136, 2008.
- [7] M. Berrada. *Une approche variationnelle de l’inversion, de la recherche locale à la recherche globale par carte topologique: application en inversion géoacoustique*. Ph.D. thesis, UPMC, France, 2008.
- [8] J. Brajard, C. Jamet, C. Moulin, and S. Thiria. Use of a Neuro-variational Inversion for Retrieving Oceanic and Atmospheric Constituents from Satellite Ocean Colour Sensor: Application to Absorbing Aerosols. *Neural Networks*, 19(2):178–185, 2006.
- [9] A. Kane, S. Thiria, and C. Moulin. Développement d’une Méthode d’Assimilation de Données in Situ dans une Version 1D du Modèle de Biogochimie Marine PISCES. Master’s thesis, LSCE/IPSL, CEA-CNRS-UVSQ, 2006.
- [10] G. Madec. *NEMO ocean engine*. Note du Pôle de modélisation de l’Institut Pierre-Simon Laplace No 27, LOCEAN, Paris, France, 2008.
- [11] YAO. Trac Page, 2016. <http://forge.ipsl.jussieu.fr/yao>.
- [12] A. Darte, Y. Robert, and F. Vivien. *Scheduling and automatic parallelization*. 2000.

- [13] K. Kennedy and K. McKinley. Typed fusion with applications to parallel and sequential code generation. Technical report, 1993.
- [14] R. Allen, D. Callahan, and K. Kennedy. Automatic decomposition of scientific programs for parallel execution. In *POPL '87: Proceedings of the 14th ACM SIGACT-SIGPLAN symposium on Principles of programming languages*, pages 63–76, NY, USA, 1987. ACM.
- [15] H. Jin, M. A. Frumkin, and J. Yan. Automatic Generation of OpenMP Directives and Its Application to Computational Fluid Dynamics Codes. In *ISHPC*, pages 440–456. Springer-Verlag, 2000.
- [16] J. Taillard, F. Guyomarc’h, and J.-L. Dekeyser. A Graphical Framework for High Performance Computing Using An MDE Approach. In *Proceedings of the 16th Euromicro Conference on Parallel, Distributed and Network-Based Processing, PDP*, pages 165–173, USA, 2008. IEEE CS.
- [17] U. Bondhugula, A. Hartono, J. Ramanujam, and P. Sadayappan. A practical automatic polyhedral parallelizer and locality optimizer. In *PLDI*, pages 101–113, USA, 2008. ACM SIGPLAN.
- [18] L. Nardi, F. Badran, P. Fortin, and S. Thiria. YAO: a generator of parallel code for variational data assimilation applications. In *IEEE 14th International Conference on High Performance Computing and Communications, HPCC-2012*, pages 224–232, june 2012.
- [19] Alfred V. Aho, Monica S. Lam, Ravi Sethi, and Jeffrey D. Ullman. *Compilers: Principles, Techniques, and Tools*. Addison Wesley, 2de edition, August 2006.